Solution Synthesized p -Type Copper Gallium Oxide Nanoplates as Hole Transport Layer for Organic Photovoltaic Devices

ARTICLE *in* JOURNAL OF PHYSICAL CHEMISTRY LETTERS · MARCH 2015

Impact Factor: 7.46 · DOI: 10.1021/acs.jpclett.5b00236

6 AUTHORS, INCLUDING:

Diego Barrera
University of Texas at Dallas
6 PUBLICATIONS **14** CITATIONS
SEE PROFILE

Liang Xu
University of Texas at Dallas
7 PUBLICATIONS **18** CITATIONS
SEE PROFILE

Yun-Ju Lee
University of Texas at Dallas
60 PUBLICATIONS **1,797** CITATIONS
SEE PROFILE

Weihua Hsu
Samsung
768 PUBLICATIONS **20,535** CITATIONS
SEE PROFILE

THE JOURNAL OF PHYSICAL CHEMISTRY Letters

Letter

pubs.acs.org/JPCL

Solution Synthesized *p*-Type Copper Gallium Oxide Nanoplates as Hole Transport Layer for Organic Photovoltaic Devices

Jian Wang,[†] Vanessa Ibarra,[†] Diego Barrera,[†,‡] Liang Xu,[†] Yun-Ju Lee,[†] and Julia W. P. Hsu*[,†]

[†]Department of Materials Science and Engineering, University of Texas at Dallas, 800 West Campbell Road, Richardson, Texas 75080, United States

[‡]Centro de Investigación en Materiales Avanzados, S.C. (CIMAV), Unidad Monterrey Alianza Norte 202, 66600 Apodaca, Nuevo León, México

Supporting Information

ABSTRACT: *p*-Type metal-oxide hole transport layer (HTL) suppresses recombination at the anode and hence improves the organic photovoltaic (OPV) device performance. While NiO_x has been shown to exhibit good HTL performance, very thin films (<10 nm) are needed due to its poor conductivity and high absorption. To overcome these limitations, we utilize $CuGaO_2$, a *p*-type transparent conducting oxide, as HTL for OPV devices. Pure delafossite phase $CuGaO_2$ nanoplates are synthesized via microwave-assisted hydrothermal reaction in a significantly shorter reaction time compared to via conventional heating. A thick $CuGaO_2$ HTL (~280 nm) in poly(3-hexylthiophene):[6,6]-phenyl-C61-butyric acid methyl ester (P3HT:PCBM) devices achieves 3.2% power conversion efficiency, on par with devices made with standard HTL materials. Such a thick $CuGaO_2$ HTL is more compatible with large-area and high-volume printing process.

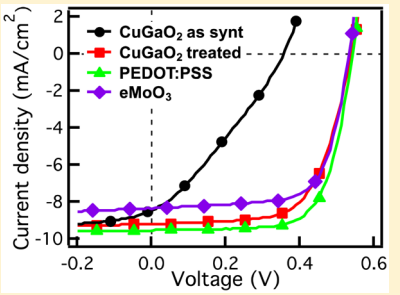

Metal oxides have been investigated as promising hole transport layers (HTLs) for organic photovoltaic (OPV) devices, because of their versatile optical and electrical properties and good physical and chemical stability.[1,2] Commonly used metal oxide HTLs include MoO_x,[3] WO_3,[4] and V_2O_5,[5] which exhibit high work function but are *n*-type semiconductor[2] and hence do not block electron transport to the anode, leading to higher recombination.[6] Thus far, only a few *p*-type metal oxides, such as NiO_x,[7−9] $Ni_xCo_{3-x}O_4$,[10] and CuO_x,[11] have been examined. While NiO_x in particular shows promising performance,[7−9,12,13] its low conductivity and high absorption coefficient require very thin films (5−10 nm).[7−9] Deposition of such a thin layer without pinholes is very challenging, particularly when using nonvacuum based techniques prevalent in industrial fabrication.[14] Therefore, it is highly advantageous to develop a thick *p*-type HTL that has high performance. Such an application requires high conductivity and transparency, similar to those for *p*-type transparent conducting oxides (TCO).[15,16]

In this paper, we report microwave-assisted synthesis of *p*-type $CuGaO_2$ crystalline nanoplates, a delafossite $Cu^{1+}M^{3+}O_2$ compound, and for the first time examine their performance as HTL in OPV devices. Delafossite nanostructures synthesized via low-temperature hydrothermal reaction have been shown as a promising alternative for NiO_x nanoparticles as photocathodes for *p*-type dye sensitized solar cells (DSSCs), because of the higher transparency, hole diffusion coefficient, and deeper ionization energy.[17−19] As these properties match HTL criteria, we expect that they should function well in OPV devices. So far, hydrothermal synthesis of delafossite nanostructures has been limited to conventional heating.[18−20] By using microwave-assisted synthesis, we obtained pure delafossite $CuGaO_2$, without Cu_2O or CuO impurities, with only 1 h reaction time, a 50× decrease compared to published results using conventional hydrothermal growth.[18−20] When we tested a thick $CuGaO_2$ layer (~280 nm) as HTLs in poly(3-hexylthiophene):[6,6]-phenyl-C61-butyric acid methyl ester (P3HT:PCBM) OPV devices, we found that annealing at 150 °C in air or UV-ozone treatment improves the device open-circuit voltage (V_{oc}), fill factor (FF), and PCE to values comparable to a device with poly(3,4-ethylenedioxythiophene):poly(styrenesulfonate) (PEDOT:PSS) HTL, and superior to a device with *n*-type MoO_3. The performance improvement can be attributed to higher work function and/or ionization energy of $CuGaO_2$ arising from oxygen incorporation.

$CuGaO_2$ nanoplates are synthesized based on a recipe modified from Srinivasan and co-workers.[20] Figure 1a shows the X-ray diffraction (XRD) spectrum of the as synthesized product, which matches the pure $CuGaO_2$ phase (PDF#00-041-0255) without other impurities. Using the well-known Scherrer equation,[18] we calculate the nanoplate thickness from (003) and (006) peak widths to be 10.3 and 8.5 nm, respectively. These values are consistent with the 10−20 nm nanoplate thickness observed in electron microscopy (Figure 1b,c and Supporting Information Figure S1a). The lower

Received: February 3, 2015
Accepted: March 9, 2015

DOI: 10.1021/acs.jpclett.5b00236
J. Phys. Chem. Lett. 2015, 6, 1071−1075

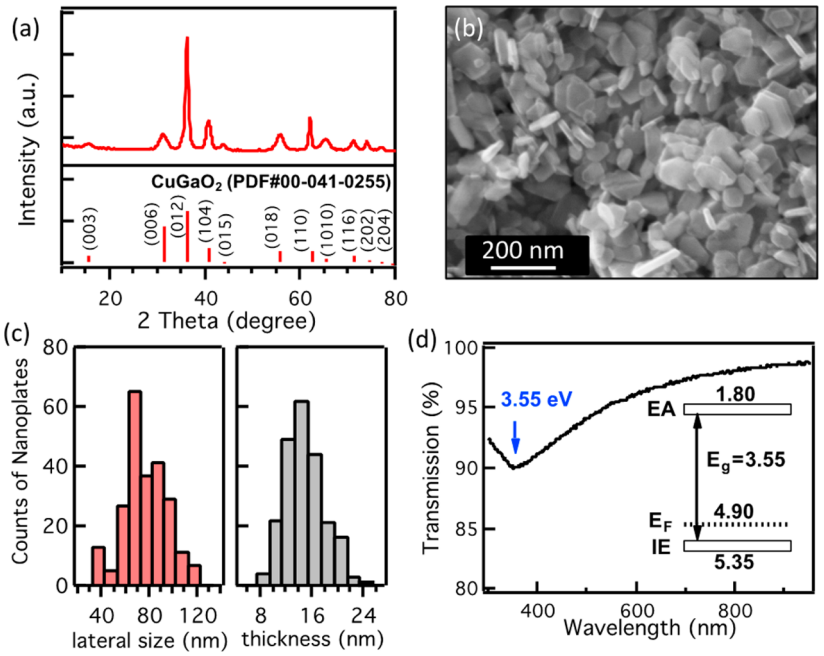

Figure 1. (a) XRD spectrum of $CuGaO_2$ nanoplates and reference powder diffraction file. (b) SEM image of a $CuGaO_2$ film. (c) Histogram of lateral size and thickness of $CuGaO_2$ nanoplates analyzed from SEM images. (d) Optical transmission spectrum of a ~280 nm $CuGaO_2$ film. Inset: $CuGaO_2$ energy diagram: IE determined by PESA, E_F determined by kelvin probe.

relative intensity of (003) and (006) peaks compared to the reference file suggests that these nanoplates preferentially exhibit an edge-on orientation with respect to the substrate. The lattice spacing of 2.65 Å measured from high-resolution transmission electron microscopy (Figure S1b) corresponds to (110) plane of $CuGaO_2$. An earlier study suggests that the synthesis of $CuGaO_2$ involves the nucleation and growth of Cu_2O seeds at lower temperature, followed by diffusion of Ga^{3+} ion into the Cu_2O lattice to form $CuGaO_2$.[18] Therefore, conventional hydrothermal reaction based on convection heating produces Cu_2O impurity because of the thermal gradient between the vessel walls and center, and requires a long reaction time to ensure full Ga^{3+} incorporation. In contrast, microwave-assisted synthesis heats up the reaction solution rapidly and uniformly.[21] Hence, high product purity is achieved at a significantly shorter reaction time (~1 h versus ~50 h). Moreover, recent research efforts have been focused on decreasing the delafossite nanoplate size.[17−20] Using microwave-assisted synthesis, we achieve $CuGaO_2$ nanoplates with dimensions 50−100 nm wide and 10−20 nm thick (Figures 1b,c and S1a), smaller compared to the 200−300 nm wide and 20−45 nm thick nanoplates from conventional heating.[18−20]

Figure 1d shows the optical transmission spectrum measured for a ~280 nm thick (Figure S2) $CuGaO_2$ film spin coated on glass. The thick film exhibits good transparency (>90% transmission) between 300 and 950 nm. An exciton absorption peak is observed at 350 nm, corresponding to an optical bandgap of 3.55 eV. This absorption peak and optical bandgap are consistent with reported values in literatures.[20,22] With the ionization energy (5.35 eV, Figure S3) measured from photoelectron spectroscopy in air (PESA) and the optical bandgap, $CuGaO_2$ electron affinity is calculated to be 1.80 eV. Kelvin probe measurement shows a work function of 4.90 eV, confirming that it is a *p*-type semiconductor. The energy level diagram is summarized in the inset of Figure 1d. Since $CuGaO_2$ has a deeper ionization energy than common donor materials such as P3HT (4.65 eV) and poly[N-9′-hepta-decanyl-2,7-carbazole-alt-5,5-(4′,7′-di-2-thienyl- 2′,1′,3′-enzothiadiazole)] (PCDTBT, 5.30 eV) and a shallower electron affinity than common acceptor materials such as PCBM (3.80 eV) and indene-C_{60} bisadduct (ICBA, 3.57 eV),[6,23] it should extract holes efficiently and block electrons to the anode.

Next, we fabricate conventional P3HT:PCBM devices with $CuGaO_2$ nanoplates as the HTL. Figure 2a shows that the as-synthesized $CuGaO_2$ HTL results in poor V_{oc}, FF, and PCE (Table 1). However, when the $CuGaO_2$ film is annealed in air at 150 °C or treated with UV-ozone, both V_{oc} and FF improve substantially, and a ~3.2% PCE is achieved. As a reference, a $CuGaO_2$ film annealed at 150 °C in N_2 shows similar device performance as the as-synthesized $CuGaO_2$ film. All devices regardless of treatment exhibit similar short-circuit current density (J_{sc}).

Figure 3a shows the effects of air annealing and UV−ozone treatment on the ionization energy and work function of $CuGaO_2$ films. Annealing in air increases work function, while UV−ozone treatment increases both ionization energy and work function of the $CuGaO_2$ film. The improvement of device performance using $CuGaO_2$ films processed under these conditions is attributed to the higher HTL work function, similar to published results.[7,12] In contrast, annealing in N_2 has no effect on either value or device performance. This result indicates that the oxygen presence in the treatment is critical to altering $CuGaO_2$ electronic properties.

To elucidate the role of oxygen on the modification of energy levels, we performed X-ray photoelectron spectroscopy (XPS) on as synthesized, air annealed, and UV−ozone treated $CuGaO_2$ films. Figure S5 and Figure 3b show that Ga 2p3/2 and Cu 2p3/2 peaks are located at 1118.0 and 932.7 eV for all three $CuGaO_2$ films. These binding energy values correspond to Ga^{3+} and Cu^{1+} states,[24] and are consistent with reported values for $CuGaO_2$ compound.[25] On the UV−ozoned film, an extra peak corresponding to $Cu(OH)_2$ is observed at 935.4 eV,

DOI: 10.1021/acs.jpclett.5b00236
J. Phys. Chem. Lett. 2015, 6, 1071−1075

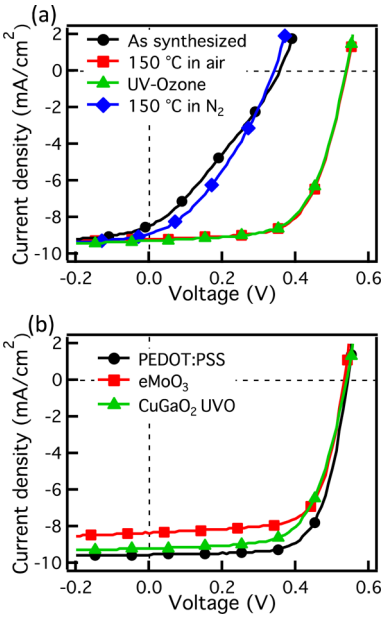

Figure 2. $J-V$ characteristics under AM 1.5G 100 mW/cm^2 illumination for conventional OPV devices with HTLs of (a) $CuGaO_2$: as-synthesized (black circle), 150 °C in air (red square), UV-ozone (green triangle), and 150 °C in N_2 (blue diamond), and of (b) PEDOT:PSS (black circle), evaporated MoO_3 (red square), and $CuGaO_2$, UV-ozone (green triangle). For comparison, $J-V$ curves of devices with PEDOT:PSS and $eMoO_3$ HTL after air-annealing or UV-ozone treatment are shown in Figure S4. The device structure is ITO (150 nm)/HTL/P3HT:PCBM (220 nm)/Ca (7 nm)/Al (100 nm).

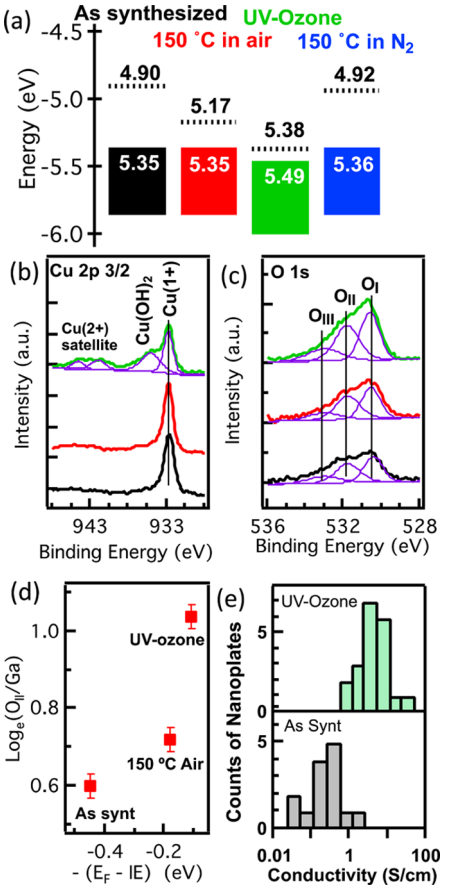

Figure 3. (a) Ionization energy and work function for $CuGaO_2$ films with different treatments. XPS spectra of (b) Cu 2p3/2, and (c) O 1s for as-synthesized (black), 150 °C annealed in air (red), and UV–ozoned (green) $CuGaO_2$ film. Purple lines represent fitted peaks. (d) Natural logarithm of O_{II}/ Ga 2p3/2 intensity ratio vs $-(E_F - IE)$, the energy difference between the work function and the ionization energy. (e) Histogram of c-axis conductivities for as synthesized or UV–ozoned $CuGaO_2$ nanoplates measured from CAFM. All conductivity data are shown in Table S1.

but no CuO peak around 933.5–934.0 eV is observed.[24] This suggests that UV–ozone treatment oxidizes the Cu species near surface, consistent with the appearance of two satellite peaks at 942–945 eV, indicating the presence of Cu^{2+} species.[25] It has been shown that oxygen plasma treatment oxidizes NiO_x and produces NiOOH species near its surface, which serves as a surface dipole to increase the film ionization energy and work function.[13] The $Cu(OH)_2$ species is likely responsible for the increase of ionization energy specific to UV–ozone treated $CuGaO_2$ film.

The O 1s signal (Figure 3c) for all three films consists of three species: the lattice oxygen of $CuGaO_2$ film (O_I) at 530.5 eV,[25] the chemisorbed or dissociated oxygen or hydroxyl species (O_{II}) at 531.8 eV,[13,25,26] and absorbed water or carbonaceous species (O_{III}) at 533.1 eV.[10,13] According to first-principle calculation, the oxygen interstitials are the main source for hole carriers in $CuGaO_2$ films.[27] Experimentally, it has also been reported that the $CuGaO_2$ films prepared via pulsed laser deposition at higher oxygen partial pressure show higher hole carrier concentrations and conductivity.[28] Therefore, we postulate that the oxygen presence in air annealing or UV-ozone treatment increases the hole concentrations in $CuGaO_2$ film via oxygen interstitial doping, which is expected to exhibit an increased O_{II} species (i.e., dissociated oxygen).[26] Because the hole concentration is proportional to $\exp^{-(E_F - IE)/kT}$ for a nondegenerate semiconductor, where E_F is Fermi level position (i.e., work function), IE is ionization energy, k is Boltzmann constant, and T is temperature, an increased hole concentration should result in a E_F value closer

Table 1. Device Characteristics with Different HTLs Shown in Figure 2[a]

HTL	processing	V_{oc} [mV]	J_{sc} [mA/cm^2]	FF	η [%]	R_s [Ω cm^2]
$CuGaO_2$	as synthesized	355 ± 29	8.46 ± 0.31	0.30 ± 0.02	0.91 ± 0.16	5.1 ± 0.5
	150 °C in Air	540 ± 6	9.18 ± 0.05	0.65 ± 0.01	3.20 ± 0.04	3.5 ± 0.8
	UV-ozone	538 ± 4	9.27 ± 0.12	0.63 ± 0.01	3.15 ± 0.07	2.9 ± 0.8
	150 °C in N_2	343 ± 25	8.89 ± 0.14	0.36 ± 0.02	1.09 ± 0.13	5.0 ± 1.2
PEDOT:PSS		540 ± 0	9.53 ± 0.37	0.70 ± 0.01	3.59 ± 0.10	2.5 ± 0.7
$eMoO_3$		532 ± 4	8.34 ± 0.08	0.69 ± 0.01	3.07 ± 0.05	2.8 ± 0.7

[a]The area of each device diode is 0.11 cm^2. A 2.5 mm diameter aperture was applied to define the illumination area of 0.049 cm^2. The ± values represent standard deviation of device parameters for at least 6 diodes per HTL condition.

DOI: 10.1021/acs.jpclett.5b00236
J. Phys. Chem. Lett. 2015, 6, 1071–1075

to IE value.[29] Figure 3d shows that the natural logarithm of O_{II}/Ga intensity ratio increases with the $-(E_F - IE)$ value, following the treatment order of as synthesized < air annealing < UV−ozone. We use the Ga 2p3/2 signal as a reference because its peak position and shape remain unchanged before and after treatments (Figure S5). This result confirms our hypothesis that increased O_{II} species, including oxygen interstitials, are responsible for the increased hole concentrations, hence the film work function. The deviation from a strict linear dependence is probably due to that the UV-ozoned $CuGaO_2$ sample has surface $Cu(OH)_2$ species (Figure 3b), which also contribute to the O_{II} signal.

Additionally, we evaluate the conductivity of individual $CuGaO_2$ nanoplates (Figure S6) using conductive atomic force microscopy (CAFM). The median conductivity value for as synthesized $CuGaO_2$ nanoplates is 0.19 S/cm. We note that such a value is 4−5 orders of magnitude higher than that reported in a previous study on conventionally synthesized $CuGaO_2$ nanoplate films using impedance spectroscopy in a planar device structure.[30] This difference likely originates from (1) CAFM measures higher current density compared to macroscopic measurements because of higher electric field at the probe−surface contact,[31] and (2) while CAFM measures individual $CuGaO_2$ nanoplates in *c*-axis, the impedance measurement was done on a porous $CuGaO_2$ nanoplate film of 1−2 μm thickness,[30] in which carrier transport could be greatly hindered by particle−particle contacts and is averaged over all crystallographic directions. After UV-ozone treatment, the median conductivity value of $CuGaO_2$ nanoplates is 3.6 S/cm, exhibiting ∼20 times increase over the as synthesized $CuGaO_2$ value (Figure 3e). Such a conductivity increase confirms the hypothesis above that oxygen incorporation increases the hole density and work function of $CuGaO_2$ nanoplates.

Finally, Figure 2b shows that OPV device with the UV-ozone treated $CuGaO_2$ HTL exhibit higher J_{sc} than evaporated MoO_3 HTL, consistent with suppression of recombination at the anode with *p*-type HTL.[6] On the other hand, $CuGaO_2$ HTL shows slightly lower FF than PEDOT:PSS HTL. This could be due to the rough $CuGaO_2$ film (Figures 1b and S7). A previous report documents that rougher ZnO film result in lower FF in an inverted OPV device.[32] Fabrication of PCDTBT:PC_{70}BM devices (∼70 nm active layer) or thin (100 nm) P3HT:PC_{60}BM devices on such a rough $CuGaO_2$ film always results in shorted device characteristics. This issue can be overcome by synthesizing smaller $CuGaO_2$ nanoparticles so that a smoother HTL film can be made. Notably, the series resistances (R_s) for device with all three HTLs are comparable (Table 1), albeit with a much thicker $CuGaO_2$ layer compared with PEDOT:PSS (∼7 times) and $eMoO_3$ (∼50 times), highlighting good OPV performance using *p*-type TCO as the HTL at practical thickness.

In conclusion, we have demonstrated that microwave-synthesized $CuGaO_2$ nanoplates function as promising HTLs for OPV devices. Air-annealing or UV−ozone treatments are critical to improve the film's work function and conductivity, and hence device performance. To further improve the device performance and to be compatible with high-performance thin active layer OPV systems, we need to reduce the film roughness by synthesizing smaller $CuGaO_2$ nanoparticles, or exploring other delafossite compounds, such as $CuAlO_2$ and $CuCrO_2$.

■ ASSOCIATED CONTENT

Supporting Information

The Supporting Information includes detailed experimental description of $CuGaO_2$ synthesis, characterization, and the OPV device fabrication. It also includes the TEM images of $CuGaO_2$ nanoplates, the ionization energy measurement using PESA, a typical AFM 3D image for the $CuGaO_2$ film prepared for device, the thickness measurement using AFM for the same film, the XPS spectra of Ga 2p3/2 signal for $CuGaO_2$ films, the CAFM measurement on individual $CuGaO_2$ nanoplates, and the *J*−*V* plot of devices with PEDOT:PSS or $eMoO_3$ HTL after annealing/UV-ozone treatment. This material is available free of charge via the Internet at http://pubs.acs.org.

■ AUTHOR INFORMATION

Corresponding Author

*E-mail: jwhsu@utdallas.edu.

Notes

The authors declare no competing financial interest.

■ ACKNOWLEDGMENTS

This project is sponsored by National Science Foundation (NSF) DMR-1305893 and the University of Texas at Dallas. D.B. acknowledges the funding support from Consejo Nacional de Ciencia y Tecnologia (CONACyT) and Project NL-2010-C33-149216, J.W.P.H. acknowledges the support from Texas Instruments Distinguished Chair in Nanoelectronics. J.W. acknowledges Dr. Xiaoye Qin for the fruitful discussion on XPS data analysis.

■ REFERENCES

(1) Shrotriya, V.; Li, G.; Yao, Y.; Chu, C.-W.; Yang, Y. Transition Metal Oxides as the Buffer Layer for Polymer Photovoltaic Cells. *Appl. Phys. Lett.* **2006**, *88*, 073508.

(2) Greiner, M. T.; Helander, M. G.; Tang, W.-M.; Wang, Z.-B.; Qiu, J.; Lu, Z.-H. Universal Energy-Level Alignment of Molecules on Metal Oxides. *Nat. Mater.* **2011**, *10*, 1−6.

(3) Lee, Y.-J.; Yi, J.; Gao, G. F.; Koerner, H.; Park, K.; Wang, J.; Luo, K.; Vaia, R. A.; Hsu, J. W. P. Low-Temperature Solution-Processed Molybdenum Oxide Nanoparticle Hole Transport Layers for Organic Photovoltaic Devices. *Adv. Energy Mater.* **2012**, *2*, 1193−1197.

(4) Stubhan, T.; Li, N.; Luechinger, N. A.; Halim, S. C.; Matt, G. J.; Brabec, C. J. High Fill Factor Polymer Solar Cells Incorporating a Low Temperature Solution Processed WO_3 Hole Extraction Layer. *Adv. Energy Mater.* **2012**, *2*, 1433−1438.

(5) Zilberberg, K.; Trost, S.; Meyer, J.; Kahn, A.; Behrendt, A.; Lützenkirchen-Hecht, D.; Frahm, R.; Riedl, T. Inverted Organic Solar Cells with Sol−Gel Processed High Work-Function Vanadium Oxide Hole-Extraction Layers. *Adv. Funct. Mater.* **2011**, *21*, 4776−4783.

(6) Ratcliff, E. L.; Zacher, B.; Armstrong, N. R. Selective Interlayers and Contacts in Organic Photovoltaic Cells. *J. Phys. Chem. Lett.* **2011**, *2*, 1337−1350.

(7) Steirer, K. X.; Ndione, P. F.; Widjonarko, N. E.; Lloyd, M. T.; Meyer, J.; Ratcliff, E. L.; Kahn, A.; Armstrong, N. R.; Curtis, C. J.; Ginley, D. S.; et al. Enhanced Efficiency in Plastic Solar Cells via Energy Matched Solution Processed NiO_x Interlayers. *Adv. Energy Mater.* **2011**, *1*, 813−820.

(8) Irwin, M. D.; Buchholz, D. B.; Hains, A. W.; Chang, R. P. H.; Marks, T. J. p-Type Semiconducting Nickel Oxide as an Efficiency-Enhancing Anode Interfacial Layer in Polymer Bulk-Heterojunction Solar Cells. *Proc. Natl. Acad. Sci. U.S.A.* **2008**, *105*, 2783−2787.

(9) Manders, J. R.; Tsang, S.-W.; Hartel, M. J.; Lai, T.-H.; Chen, S.; Amb, C. M.; Reynolds, J. R.; So, F. Solution-Processed Nickel Oxide Hole Transport Layers in High Efficiency Polymer Photovoltaic Cells. *Adv. Funct. Mater.* **2013**, *23*, 2993−3001.

DOI: 10.1021/acs.jpclett.5b00236
J. Phys. Chem. Lett. 2015, 6, 1071−1075

(10) Ndione, P. F.; Garcia, A.; Widjonarko, N. E.; Sigdel, A. K.; Steirer, K. X.; Olson, D. C.; Parilla, P. A.; Ginley, D. S.; Armstong, N. R.; Richards, R. E.; et al. Highly-Tunable Nickel Cobalt Oxide as a Low-Temperature p-Type Contact in Organic Photovoltaic Devices. *Adv. Energy Mater.* **2012**, *3*, 524−531.
(11) Xu, Q.; Wang, F.; Tan, Z.; Li, L.; Li, S.; Hou, X.; Sun, G.; Tu, X.; Hou, J.; Li, Y. High-Performance Polymer Solar Cells with Solution-Processed and Environmentally Friendly CuO_x Anode Buffer Layer. *ACS Appl. Mater. Interfaces* **2013**, *5*, 10658−10664.
(12) Ratcliff, E. L.; Garcia, A.; Paniagua, S. A.; Cowan, S. R.; Giordano, A. J.; Ginley, D. S.; Marder, S. R.; Berry, J. J.; Olson, D. C. Investigating the Influence of Interfacial Contact Properties on Open Circuit Voltages in Organic Photovoltaic Performance: Work Function Versus Selectivity. *Adv. Energy Mater.* **2013**, *3*, 647−656.
(13) Ratcliff, E. L.; Meyer, J.; Steirer, K. X.; Garcia, A.; Berry, J. J.; Ginley, D. S.; Olson, D. C.; Kahn, A.; Armstrong, N. R. Evidence for Near-Surface NiOOH Species in Solution-Processed NiO_x Selective Interlayer Materials: Impact on Energetics and the Performance of Polymer Bulk Heterojunction Photovoltaics. *Chem. Mater.* **2011**, *23*, 4988−5000.
(14) Stubhan, T.; Oh, H.; Pinna, L.; Krantz, J.; Litzov, I.; Brabec, C. J. Inverted Organic Solar Cells Using a Solution Processed Aluminum-Doped Zinc Oxide Buffer Layer. *Org. Electron.* **2011**, *12*, 1539−1543.
(15) Kawazoe, H.; Yanagi, H.; Ueda, K.; Hosono, H. Transparent p-Type Conducting Oxides: Design and Fabrication of p−n Heterojunctions. *MRS Bull.* **2000**, *25*, 28−36.
(16) Banerjee, A. N.; Chattopadhyay, K. K. Recent Developments in the Emerging Field of Crystalline p-Type Transparent Conducting Oxide Thin Films. *Progress in Crystal Growth and Characterization of Materials* **2005**, *50*, 52−105.
(17) Yu, M.; Draskovic, T. I.; Wu, Y. Cu(I)-Based Delafossite Compounds as Photocathodes in p-Type Dye-Sensitized Solar Cells. *Phys. Chem. Chem. Phys.* **2014**, *16*, 5026.
(18) Xu, Z.; Xiong, D.; Wang, H.; Zhang, W.; Zeng, X.; Ming, L.; Chen, W.; Xu, X.; Cui, J.; Wang, M.; et al. Remarkable Photocurrent of p-Type Dye-Sensitized Solar Cell Achieved by Size Controlled $CuGaO_2$ Nanoplates. *J. Mater. Chem. A* **2014**, *2*, 2968.
(19) Yu, M.; Natu, G.; Ji, Z.; Wu, Y. p-Type Dye-Sensitized Solar Cells Based on Delafossite $CuGaO_2$ Nanoplates with Saturation Photovoltages Exceeding 460 mV. *J. Phys. Chem. Lett.* **2012**, *3*, 1074−1078.
(20) Srinivasan, R.; Chavillon, B.; Doussier-Brochard, C.; Cario, L.; Paris, M.; Gautron, E.; Deniard, P.; Odobel, F.; Jobic, S. Tuning the Size and Color of the p-Type Wide Band Gap Delafossite Semiconductor $CuGaO_2$ with Ethylene Glycol Assisted Hydrothermal Synthesis. *J. Mater. Chem.* **2008**, *18*, 5647.
(21) Zhu, Y.-J.; Chen, F. Microwave-Assisted Preparation of Inorganic Nanostructures in Liquid Phase. *Chem. Rev.* **2014**, *114*, 6462−6555.
(22) Ueda, K.; Hase, T.; Yanagi, H.; Kawazoe, H.; Hosono, H.; Ohta, H.; Orita, M.; Hirano, M. Epitaxial Growth of Transparent p-Type Conducting $CuGaO_2$ Thin Films on Sapphire (001) Substrates by Pulsed Laser Deposition. *J. Appl. Phys.* **2001**, *89*, 1790.
(23) Guan, Z.-L.; Bok Kim, J.; Loo, Y.-L.; Kahn, A. Electronic Structure of the Poly(3-Hexylthiophene):Indene-C_{60} Bisadduct Bulk Heterojunction. *J. Appl. Phys.* **2011**, *110*, 043719.
(24) Wagner, C. D.; Riggs, W. M.; Davis, L. E.; Moulder, J. E.; Muilenberg, G. E. *Handbook of X-Ray Photoelectron Spectroscopy*, 1st ed.; Perkin-Elmer Corporation: Waltham, MA, 1979.
(25) Han, M.; Jiang, K.; Zhang, J.; Yu, W.; Li, Y.; Hu, Z.; Chu, J. Structural, Electronic Band Transition and Optoelectronic Properties of Delafossite $CuGa_{1-x}Cr_xO_2$ ($0 \le x \le 1$) Solid Solution Films Grown by the Sol−Gel Method. *J. Mater. Chem.* **2012**, *22*, 18463.
(26) Ilyas, U.; Rawat, R. S.; Tan, T. L.; Lee, P.; Chen, R.; Sun, H. D.; Fengji, L.; Zhang, S. Oxygen Rich p-Type ZnO Thin Films Using Wet Chemical Route with Enhanced Carrier Concentration by Temperature-Dependent Tuning of Acceptor Defects. *J. Appl. Phys.* **2011**, *110*, 093522.
(27) Fang, Z.-J.; Fang, C.; Shi, L.-J.; Liu, Y.-H.; Han, M.-C. First-Principles Study of Defects in $CuGaO_2$. *Chin. Phys. Lett.* **2008**, *25*, 2997.
(28) Mine, T.; Yanagi, H.; Nomura, K.; Kamiya, T.; Hirano, M.; Hosono, H. Control of Carrier Concentration and Surface Flattening of $CuGaO_2$ Epitaxial Films for a p-Channel Transparent Transistor. *Thin Solid Films* **2008**, *516*, 5790−5794.
(29) Sze, S. M.; Ng, K. K. *Physics of Semiconductor Devices*, 3rd ed.; John Wiley & Sons: New York, 2006.
(30) Herraiz-Cardona, I.; Fabregat-Santiago, F.; Renaud, A.; Julián-López, B.; Odobel, F.; Cario, L.; Jobic, S.; Giménez, S. Hole Conductivity and Acceptor Density of p-Type $CuGaO_2$ Nanoparticles Determined by Impedance Spectroscopy: the Effect of Mg Doping. *Electrochim. Acta* **2013**, *113*, 570−574.
(31) Reid, O. G.; Munechika, K.; Ginger, D. S. Space Charge Limited Current Measurements on Conjugated Polymer Films Using Conductive Atomic Force Microscopy. *Nano Lett.* **2008**, *8*, 1602−1609.
(32) Ma, Z.; Tang, Z.; Wang, E.; Andersson, M. R.; Inganäs, O.; Zhang, F. Influences of Surface Roughness of ZnO Electron Transport Layer on the Photovoltaic Performance of Organic Inverted Solar Cells. *J. Phys. Chem. C* **2012**, *116*, 24462−24468.

DOI: 10.1021/acs.jpclett.5b00236
J. Phys. Chem. Lett. 2015, 6, 1071−1075